EXPERIMENTAL INVESTIGATION OF A FLAPPING WING MODEL: SOME CHALLENGES FROM UNSTEADY AERODYNAMICS

Tatjana Hubel, Cam Tropea
Fachgebiet Strömungslehre und Aerodynamik, Technische Universität Darmstadt
Petersenstr. 30, D-64287 Darmstadt, Germany
ctropea@sla.tu-darmstadt.de, tycora@web.de

ABSTRACT

A flapping-wing model has been experimentally investigated in the large (2.2m x 2.9m), low-speed wind tunnel of the Technische Universtität Darmstadt. All tests were conducted at Reynolds numbers between 26,500 and 135,000 and throughout a range of reduced frequencies between 0.029 and 0.29, where the reduced frequency is defined as $k=(\pi fc)/U_{\infty}$ (f is the wingbeat frequency, U_{∞} the free-stream velocity, and c the average wing chord.) The relationships between flight parameters and the change in circulation during the course of a wing-beat cycle have been investigated. Particle Image Velocimetry (PIV), synchronized with the wing-beat cycle, has been used for flow field measurements and visualization. This yields the phase-averaged reconstruction of the flow field in measurement planes behind the wing parallel and perpendicular to the flow direction. This visualizes the shedding vortices from the wing trailing edge and the tip vortices in the far-field wake, respectively. The results of the flow visualization study are then used to calculate the phase resolved forces acting on the model.

INTRODUCTION

Accompanying the recent development of Micro Air Vehicles (MAVs), a keen interest in the fundamental aerodynamics of flapping flight has arisen. Simultaneously, the aerodynamics of bird and insect flight are currently being studied in great detail by biologists in an effort to understand better the interaction of mechanics, morphology and the energy budget of these species (Ellington 1999, Dickinson *et al*. 1999, Sane 2003, Rayner and Gordon 1998, Spedding *et al*. 2003). In comparison with conventional propulsion systems, flapping flight allows for a very high manoeuvrability, an important advantage when flying in confined spaces. However, to date many aerodynamic questions must still be resolved in order for flapping flight to be used in technical applications. Animal flight can contribute to our understanding of the mechanisms of flapping flight especially at low Reynolds numbers. One challenge facing such studies is the direct force measurement on swimming and flying animals, which generally will not fly or swim in an undisturbed manner when tethered. A handful of successful direct-force measurements have been made with insects such as locusts (Zarnack 1969, Cloupeau *et al*. 1979, Wilkin 1990), moths (Wilkin 1991, Wilkin and Williams 1993) and fruit flies (Dickinson and Gotz 1996) but there always remains some doubt correlating the experimental results with real-life flying or swimming behaviour. Pressure measurements on animals are similarly very complicated (Usherwood *et al*. 2003, 2005) and time consuming. Therefore the visualization of the wake structure generated by the moving animal is now being more frequently used to indirectly analyze the generated aerodynamic or hydrodynamic forces.

Recent advances in optical measurement techniques such as particle image velocimetry (PIV) allow not only a qualitative analysis (Spedding *et al*. 1986, 1987a, 1987b, Willmott *et a*l. 1997) but also a quantitative investigation of the wake in terms of the instantaneous velocity and vorticity fields (Drucker and Lauder 1999, Spedding *et a*l. 2003, Warrick *et al*. 2005). Using the control-volume approach and applying the momentum equation, it is possible to obtain the aerodynamic forces acting on the body by taking into account the total surface forces over the entire control volume. However, even in steady locomotion conditions such as in cruising flight there exists a periodic acceleration and deceleration over most, if not all of the animal's body. Because of the unsteady flow moving around the body an exact determination of aerodynamic or hydrodynamic forces requires in theory the net flow of momentum out of the control volume surface as well as the time rate of change due to the unsteady fluctuations inside the control volume itself (Dabiri 2005). In practice it is nearly impossible to measure all this information simultaneously. However, one can measure the velocity field on a two-dimensional plane out of the control volume. From this velocity field one can infer the vorticity field in the measurement plane.

In the context of bird flight, and applying Helmholtz's vortex laws, one assumes that the circulation in a closed-vortex ring is equal throughout. Therefore one can surmise that the tip-vortex circulation of a single wing should equal that of the bound vortex circulation, and thus the lift produced through the Kutta-Joukowsky theorem (Panda and Zaman 1994). Therefore depending on what measurement plane is used, one can either capture the changes in the bird's lift (observed in the circulation change in the wake on a plane parallel to the flow direction) or the total lift (measured by the circulation of the wing-tip vortex on a plane normal to the flow direction). This hypothesis is tested in the present investigation for a flapping bird model.

EXPERIMENTAL FACILITY AND METHODS

The life-sized flapping-wing model is based on the aerodynamic characteristics of a goose, with a span of 1.13m and a wing-beat frequency up to 2.2Hz. The Reynolds number was varied between 26,500 and 135,000, while the wing-motion amplitude and the angle of attack were adjusted at the shoulder joint. A realistic bird-like wing profile was not used since there exists a large discrepancy between the wing profiles of resting versus flying birds, thus a profile comparable to the proximal wing section of a gliding bird (cambered profile with rounded leading edge), a Wortmann Fx-60-126 was used exclusively across the entire wing span. The flapping amplitude is asymmetrical, where the typical extension downwards was 17° and the typical extension upwards was 27°.

In this study, particle image velocimetry (PIV) was used as a visualization tool as well as to capture the instantaneous velocity-field. Due to the large flapping amplitude (as high as 0.34m at the wing tip), the visualization domain was patched together using multiple camera positions. A 200mJ Nd:YAG double-pulse laser (New Wave Gemini 200) was used for illumination, producing a pulse width of 10ns and a variable duration between pulses. Images were taken with a CCD camera (PCO SensiCam, 1024x1280Pixel). All further processing was performed using the standard two-dimensional PIV software system from Dantec Dynamics (Flow Manager®). The first image in the wing-beat cycle was triggered via a rotational potentiometer in the model, while all subsequent images were triggered via pre-set time stepping. Because of the low-pulse frequency of the laser, the wing-beat cycle was reconstructed as a phase-averaged flow field. However, it should be noted that this phase-averaging produces a pseudo time-resolved flow field, since sampling has been ensemble averaged over many (25-50) wing-beat cycles. Furthermore, for each wing-beat cycle, 50 to 70 positions were sampled depending on the wing-beat frequency. For the case of the static wing measurements, in which the wings were fixed in the horizontal position, 500 image pairs were sampled and then averaged.

The vorticity (ω) in the observation area was calculated from the vector field in the following manner:

$$\omega_x = \frac{\partial w}{\partial y} - \frac{\partial v}{\partial z} \text{ (streamwise)}; \quad \omega_y = \frac{\partial u}{\partial z} - \frac{\partial w}{\partial x} \text{ (transverse)} \qquad (1)$$

The circulation (Γ) over the measurement plane is calculated through integration of the vorticity in the following manner:

$$\Gamma = \iint_A \omega \, dA \qquad (2)$$

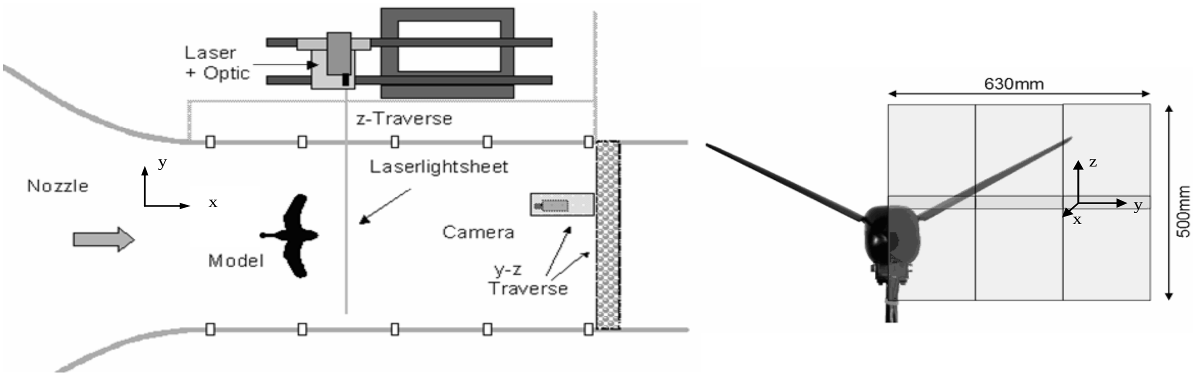

Figure 1: Measurement planes and patches used for flow field measurements perpendicular to the flow direction

Measurements in the tip-vortex plane

The laser light sheet was positioned 2.2c downstream of the trailing edge, thus there is a phase shift between wing amplitude and the flow field in the observation area (Fig. 1). In order to correlate the flow field and the wing-amplitude position, the free-stream velocity was taken to be the convective velocity as in Lee und Lee (2006). Fig. 2 shows the normalized circulation calculated from the plane perpendicular to the flow stream over the wing-beat cycle before and after the phase-shift correction for a Reynolds number of 26,500

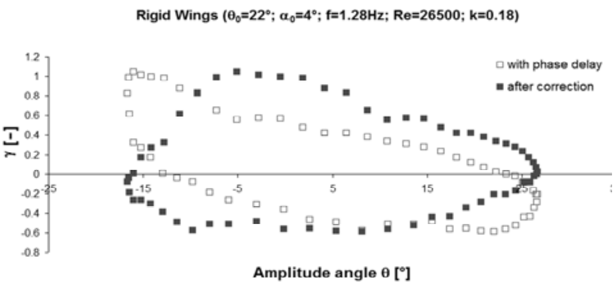

Figure 2: Normalized circulation calculated from the tip-vortex plane with and without phase-shift correction based on the freestream velocity.

To calculate the circulation, the integration of the vorticity over the entire observation area has been performed. To obtain information about the distribution of the circulation, the observation area was separated in small strips (Fig. 3) and the circulation of each strip was calculated in order to obtain the change in circulation over the span. The circulation was derived from the vorticity field by integration over the strip area (A_i):

$$\Delta\Gamma_i = \iint_A \omega_{x,i} dA_i \qquad (3)$$

The change in circulation was normalized with the free-stream velocity (U_∞) and the average wing chord (c):

$$\Delta\gamma_i = \frac{\Delta\Gamma_i}{U_\infty c} \qquad (4)$$

In order to obtain the distribution of the circulation in the observation area the change in circulation was summed over the wing span, in the following manner:

$$\gamma_i = \sum_{j=1}^{i} \Delta\gamma_j \qquad (5)$$

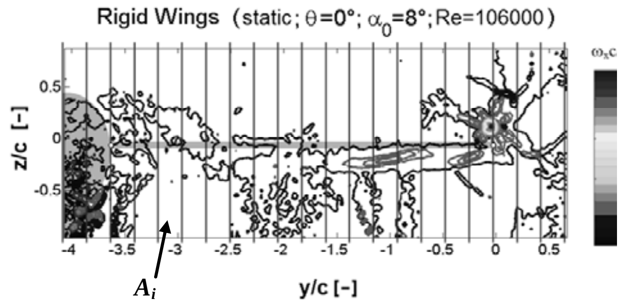

Fig. 3: Contours of normalized vorticity illustrated over partitioned observation area behind the wing (tip-vortex plane).

Measurements in the transverse vortex plane

In order to visualize the traverse vortices, PIV measurements were performed at several wing span positions parallel to the flow direction, as illustrated in Fig. 4.

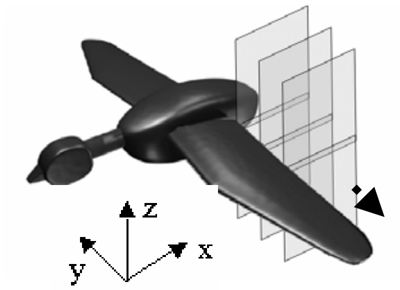

Figure 4: Measurement planes and patches used for flow field measurements parallel to the flow direction

The approximate change of circulation in the spanwise direction was measured. This was performed by calculating the vorticity contained in the start/stop vortices leaving the trailing edge over each measurement plane. The change of bound circulation on the wing occurring during the time interval $\Delta t = t_{i+1} - t_i$ is given by the integral:

$$\Delta\Gamma = \oint_{C_{i+1}} \vec{v} d\vec{l} = \iint_{A_{i+1}} \omega_y dA \qquad (6)$$

where the contour C_{i+1} or area A_{i+1} are given by the material lines defined by fluid elements originating from a fixed reference line placed immediately downstream of the trailing edge. This procedure is sketched in Fig. 5.

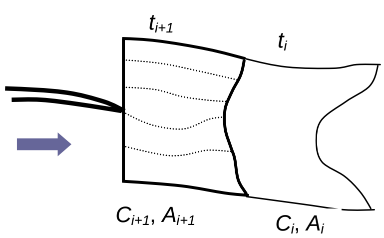

Figure 5: Wake integration contours for computing circulation change: Lagrangian particle tracking.

However these contours can only be experimentally obtained using time-resolved acquisition of the wake-velocity field and a corresponding Lagrangian particle tracking. An approximation is to use only the streamwise velocity component defining the downstream contour of the area, i.e.

$$d(z) = \frac{\left[u_i(z) + u_{i+1}(z)\right]}{2}\Delta t, \qquad (7)$$

where u_i and u_{i+1} are the velocities at the upstream and downstream end of the integration area. The choice of Δt is also limited by the number of images N over one wing-beat period T, i.e. $\Delta t = T/N$.

RESULTS

Tip-Vortex Plane

Fig. 6 shows the distribution of the normalized circulation over the span for different positions over the wing-beat cycle at different reduced frequencies and Reynolds numbers. The areas behind the body and the sting were problematic because of the significant levels of turbulence associated with the wing-body interaction. The standard deviation of the calculated circulation was high (depending on velocity and flapping frequency) in the wing-body region of the observation area. There is a decrease in the circulation in the body area and it is assumed that this is caused by the gap between the body and the wing (flow leakage), which is necessary to allow for relative movement between the two.

The diagrams show the distribution of the circulation at the upper and lower reversal points as well as for the instant when they pass through the horizontal position during the upstroke and downstroke. Generally the highest lift is generated during the downstroke whereas the lowest lift is produced during the upstroke. At the reversal points the distribution is quite similar to one another, an interesting observation considering that the phase delay of the circulation as well as the asymmetrical amplitude should play a role. At a low reduced frequency of 0.04 there is a positive lift generation over almost the entire wing-beat cycle. The distribution at k=0.09 on the other hand shows that during the upstroke, the part of the wing close to body produces positive lift whereas the distal region generates negative lift. At high reduced frequencies, for example k=0.14, the wing generates negative lift in the horizontal position during the upstroke.

Some indication of separation in the wing tip region is apparent when the development of normalized circulation as a function of wing position (amplitude angle) on the downstroke is examined, as given in Fig. 7 for a low (a: k=0.04) and high (b: k=0.14) reduced frequency. The distribution has now been given as a function of wing-fixed span coordinate (y') due to the circular arch movement the wing makes.

The upper and lower reversal points have been included in these diagrams: for low reduced frequencies these two wing positions correspond to the flow state most similar to the non-flapping condition and, indeed, they are very similar and follow closely the wing plan form area (solid curve). At higher reduced frequencies a clear difference is seen between the upper and lower reversal points, indicating the phase shift of the flow development over the wing position.

At low reduced frequencies the circulation increases at the wing tip more than at the root, a result of the higher effective angle of attack (AOA), but the general shape of the normalized circulation over the wing span does not change significantly. However, at high reduced frequencies a different behavior is observed. Until the horizontal position (maximum effective AOA) the circulation rises linearly from the root to the tip, explained by the increased effective AOA. The second half of the downstroke exhibits a rather flat distribution of circulation, with a more localized peak shifted from the tip towards the root. This is a clear indication of flow separation which then propagates from the tip to the root. This also explains the much larger difference between the circulation distribution at the upper and lower reversal points.

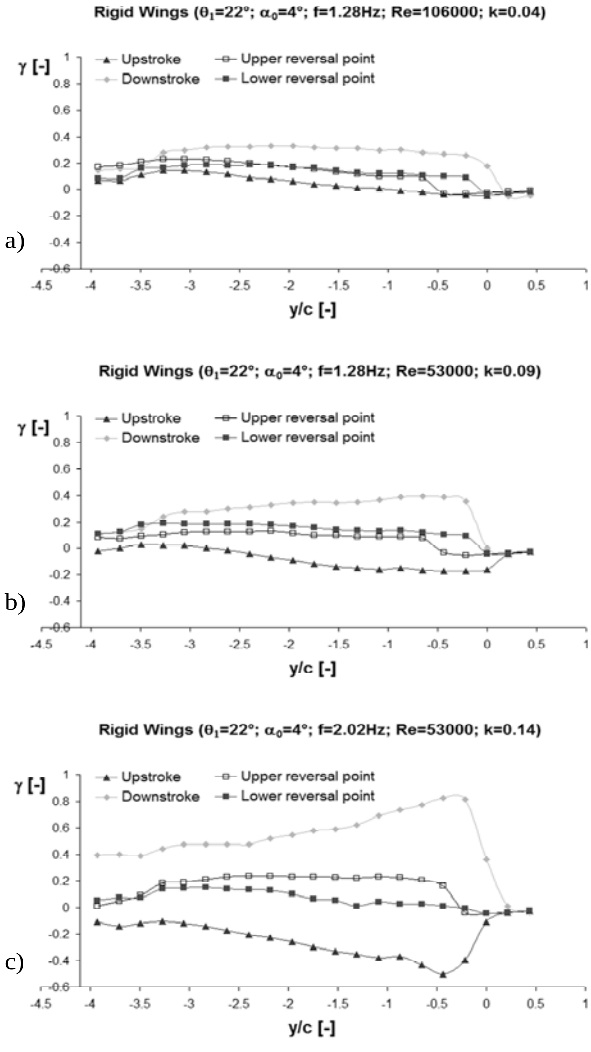

Figure 6: Distribution of normalized circulation over the span in the wake of the model at different reduced frequencies and Reynolds numbers (tip-vortex plane).

The increasing change in circulation over the wing beat cycle with increasing reduced frequency is shown in Fig. 8. In addition it can also be seen that there is a net negative lift production at higher reduced frequencies as indicated in Fig. 6b,c.

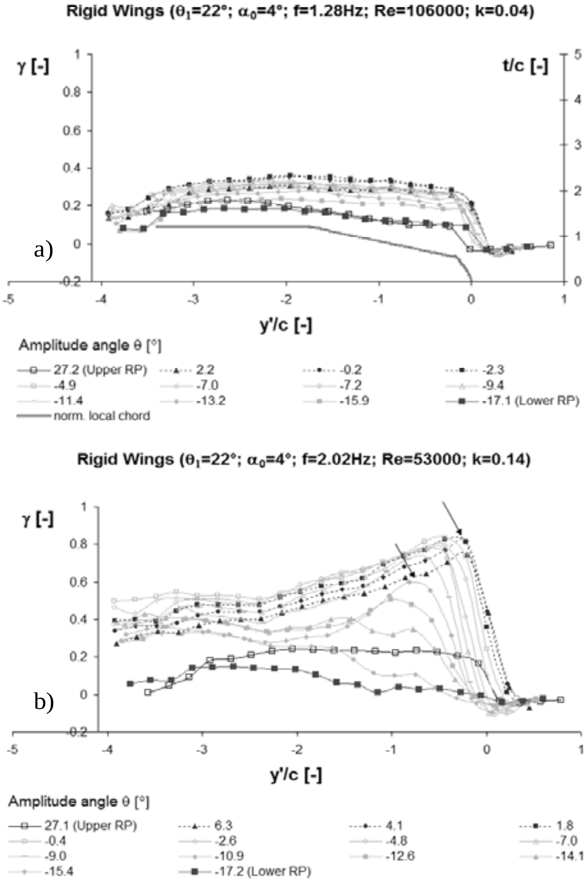

Figure 7: Distribution of normalized circulation over the span in the wake of the model at different reduced frequencies and Reynolds numbers for the downstroke (tip-vortex plane). (wing-fixed coordinate system *y'*, *t*=local chord, *c*=average chord, RP=Reversal Point)

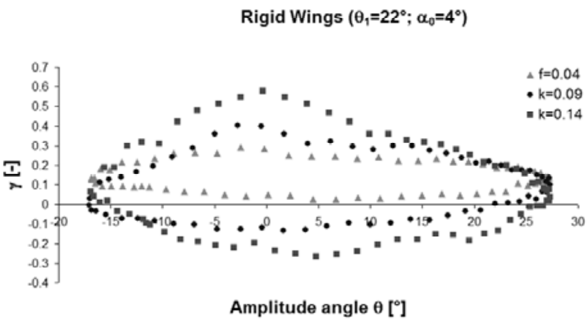

Figure 8: Normalized circulation over the wing beat cycle at different reduced frequencies and Reynolds numbers (tip-vortex plane).

Transverse Vortex Plane

The change in circulation measured in the plane parallel to the flow direction is shown in Figure 9 and 10. The variation in the circulation from the body to the wing tip can be seen in Fig. 9. A strong correlation with the amplitude angle can be seen through the positive change in circulation from the middle of the upstroke until the last third of the downstroke. This can be explained by the asymmetric flapping, the associated asymmetric effective angle of attack and the aerodynamic phase lag. A positive change in circulation in the wake is due to an increasing lift on the wing itself. There is a significant decrease in the positive change in circulation in the region of the upper reversal point as seen in Figure 7b.

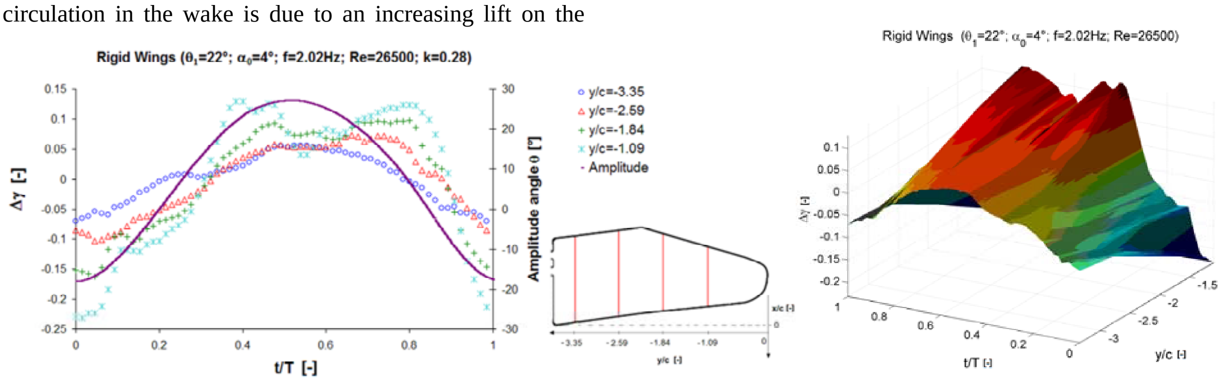

Figure 9: Change in normalized circulation over the wing-beat cycle (transverse-vortex plane) a) at different positions over the wing span in correlation with the amplitude (wing position), b) three-dimensional image of the change in circulation

A comparison with the angular acceleration of the wing in Fig. 10 shows a strong correlation between the acceleration and deceleration of the wing and the change in circulation in the wake. This reinforces the expectation that the vertical velocity of the wing and the associated change of effective angle of attack is immediately apparent in the separating transverse vortices in the wake.

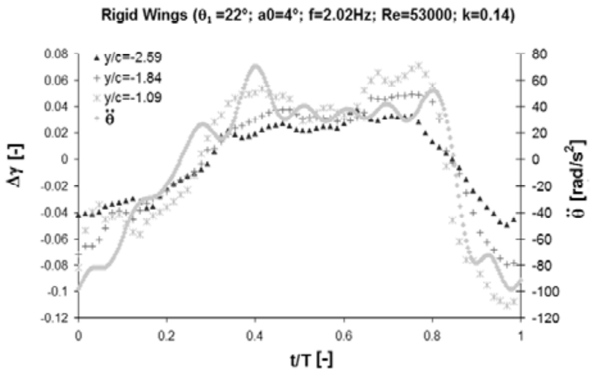

Figure 10: Change in normalized circulation over the wing-beat cycle calculated for the transverse vortex plane parallel to the flow stream at three different positions compared to the angular velocity of the wings.

To compare the results from the tip-vortex plane and the transverse-vortex plane, the change of circulation over the wing-beat cycle has been plotted Fig. 11. The change in circulation in the observation area perpendicular to the flow stream has been calculated at the same spanwise position as the images from the transverse vortices were taken; however, because of the low resolution in the tip vortex plane, a larger area has been considered (y/c=0.22). The transverse-vortex plane was limited by the thickness of the laser-light sheet at approximately 3mm. After the phase correction of the results from the tip-vortex plane, the comparison of the change of circulation obtained from the different planes show a similar magnitude and shape. The conformity depends on the Reynolds number and the reduced frequency and tends to agree better at lower reduced frequencies. The variation in the circulation from the two planes can be attributed to the fact that measurements were made in the wake and are thus not equal to the distribution directly on the wing itself; thus the tip-vortex roll-up process has an influence on the results.

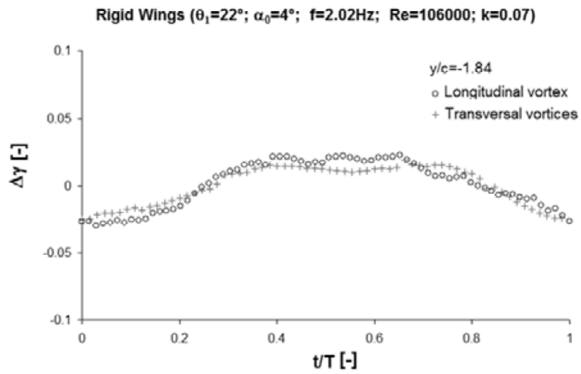

Figure 11: Change in circulation over the wing-beat cycle calculated from the tip-vortex plane (longitudinal vortex) perpendicular to the flow stream and the transverse-vortex plane (transversal vortex) parallel to the flow stream at a wing span position close to the body (y/c=-1.84).

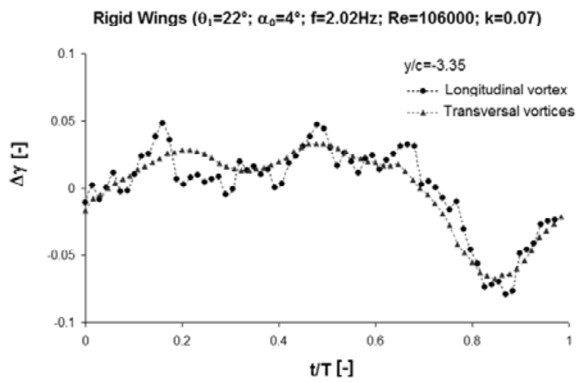

Figure 12: Change in circulation over the wing-beat cycle calculated from the tip-vortex plane (longitudinal vortex) perpendicular to the flow stream and the transverse-vortex plane (transversal vortex) parallel to the flow stream at a wing span position close to the body (y/c=-3.35).

In addition, with increasing Reynolds number and reduced frequency, the measurements close to the body (y/c=-3.35) show an increasing influence of the high turbulence and the pressure equalization due to the wing/body gap. The change in circulation at this spanwise position is very large over the wing-beat cycle, and moreover, the amplitude of the change in circulation is even more asymmetric, implying that the positive and negative circulation is not equalized at the end of the wing-beat cycle. This effect can be explained by the three-dimensional nature of the wake. Despite this highly three-dimensional flow field, the aforementioned comparison between the observation planes parallel and perpendicular to the flow stream yields reasonable agreement, as shown in Fig. 12.

CONCLUSIONS

Wake PIV measurements in two planes perpendicular to each other (streamwise and spanwise directions) have been performed. Measurements in the plane perpendicular to the flow stream allows the calculation of the total circulation on the wing itself as well as the change in circulation over the wing-beat cycle. Furthermore it has been possible to obtain the distribution of the circulation over the wing span when the observation area is close to the trailing edge. The acceptability of using wake measurements to provide the circulation distribution on the wing itself is dependent on the proximity of the measurements to the wing as well as the flow velocity, reduced frequency and the spanwise position. Furthermore, the visualization of the transverse vortices at different positions provided information on the distribution of the circulation over the wing span. However, it was found that measurements close to the body are difficult to conduct since the change in circulation in this area is usually relatively small and since there is a high level of laser light reflection. There is a strong correlation between the angular acceleration and the change in circulation over the wing-beat cycle as can be expected for quasi-steady conditions. The distribution of circulation in the wake provides clear indications of flow separation and instationary effects; however further visualization on the wing itself would be necessary to show this conclusively.

REFERENCES

Cloupeau, M., Devillers, J. F. And Devezeaux, D. ; 1979 ; "Direct Measurements of Instantaneous Lift in Desert Locust: Comparison with Jensen's Experiments on Detached Wings," J. Exp. Biol., Vol. 80, pp. 1-15.

Dabiri, J. O., 2005, "On the Estimation of Swimming and Flying Forces from Wake Measurements", J. Exp. Biol., Vol. 208, pp. 3519-3532.

Dickinson, M. H., Lehmann, F.-O. and Sane, S. P., 1999, "Wing Rotation and the Aerodynamic Basis of Insect Flight," Science, Vol. 284, pp. 1954-1960.

Dickinson, M.H. and Gotz, K.G.., 1996, "The Wake Dynamics and Flight Forces of the Fruit Fly Drosophila Melanogaster," J. Exp. Biol., Vol. 199, pp. 2085-2104.

Drucker, E. G. and Lauder, G. V., 1999, "Locomotor Forces on a Swimming Fish: Three-dimensional Vortex Wake Dynamics Quantified Using Digital Particle Image Velocimetry," J. Exp. Biol., Vol. 202, pp. 2393-2412.

Ellington C. P., 1999, "The Novel Aerodynamics of Insect Flight: Applications to Micro Air Vehicles," J. Exp. Biol., Vol. 202, pp. 3439-3448.

Lee, L. and Lee, T., 2006, "Oscillating-wing Tip Vortex with Passive Short-span Trailing-edge Strip," Journal of Aircraft, Vol. 43, No. 3, pp. 723-731.

Rayner, J. M. V., and Gordon, R., 1998, "Visualization and Modelling of the Wakes of Flying Birds,". In: Biona Report. 13, Motion Systems, ed. Blickhan, R., Wisser, A. & Nachtigall, W., pp. 165–173. Jena: Gustav Fischer Verlag.

Panda, J. and Zaman, K. M. B. Q., 1994, "Experimental Investigation of the Flow Field of an Oscillating Airfoil and Estimation of Lift from Wake Surveys," J. Fluid Mech., Vol. 265, pp. 65-95.

Sane, S. P., 2003, "Review: The Aerodynamics of Insect Flight," J. Exp. Biol., Vol. 206, pp. 4191-4208.

Spedding, G. R., 1986 "The Wake of a Jackdaw (Corvus monedula) in Slow Flight," J. Exp. Biol., Vol. 125, pp. 287–307.

Spedding, G. R., 1987a, "The Wake of a Kestrel (Falco tinnunculus) in Gliding Flight," J. Exp. Biol., Vol. 127, pp. 45–57.

Spedding, G. R., 1987b, "The Wake of a Kestrel (Falco tinnunculus) in Flapping Flight," J. Exp. Biol., Vol. 127, pp. 59–78.

Spedding, G. R. , Rosén, M. and Hedenström A., 2003 "A Family of Vortex Wakes Generated by a Thrush Nightingale in Free Flight in a Wind Tunnel over its Entire Natural Range of Flight Speeds," J. Exp. Biol., Vol. 206, pp. 2313-2344.

Usherwood, J. R., Hedrick, T. L., McGowan, C. P. and Biewener, A. A., 2005 ´"Dynamic Pressure Maps for Wings and Tails of Pigeons in Slow, Flapping Flight, and their Energetic Implications," J. Exp. Biol., Vol. 208, pp. 355-369. doi:10.1242/jeb.01359.

Usherwood, J. R., Hedrick, T. L. and Biewener, A. A., 2003,. "The Aerodynamics of Avian Take-off from Direct Pressure Measurements in Canada Geese (Branta canadensis)," J. Exp. Biol., Vol. 206, pp. 4051-4056.

Warrick, D. R., Tobalske, B. W. and Powers, D. R., 2005, "Aerodynamics of the Hovering Hummingbird,". Nature, Vol. 435, pp. 1094-1097.

Wilkin, P. J., 1990, "The Instantaneous Force on a Desert Locust, Schistocerca gregaria (Orthoptera: Acrididae), Flying in a Wind Tunnel," J. Kansas Ent. Soc., Vol. 63, pp. 316–328.

Wilkin, P. J., 1991, "Instantaneous Aerodynamic Forces Developed by an Indian Moon Moth, Actias selene, in Near Hovering Flight," Physiol. Zool., Vol. 64, pp. 193–211.

Wilkin, P. J. and Williams, M. H., 1993, "Comparison of the Instantaneous Aerodynamic Forces on a Sphingid Moth with those Predicted by Quasi-steady Aerodynamic Theory," Physiol. Zool., Vol. 66, pp. 1015–1044.

Willmott, A. P., Ellington, C. P. and Thomas, A. L. R., 1997, "Flow Visualization and Unsteady Aerodynamics in the Flight of the Hawkmoth, manduca sexta," Phil. Trans. Roy. Soc. of London B, Vol. 352(1351), pp.303–316.

Zarnack, W., 1969, „Kinematik der Flügelbewegungen bei Locusta migratoria L," Dissertation, Universität München.